Multichannel, time-resolved picosecond laser ultrasound imaging and spectroscopy with custom complementary metal-oxide-semiconductor detector

Richard J. Smith,[1] Roger A. Light,[1] Steve D. Sharples,[2] Nicholas S. Johnston,[1] Mark C. Pitter,[1] and Mike G. Somekh[1]
[1]*Institute of Biophysics, Imaging and Optical Science, University of Nottingham, Nottinghamshire NG7 2RD, United Kingdom*
[2]*Applied Optics Group, Electrical Systems and Optics Research Division, University of Nottingham, Nottinghamshire NG7 2RD, United Kingdom*

(Received 19 October 2009; accepted 5 January 2010; published online 4 February 2010)

This paper presents a multichannel, time-resolved picosecond laser ultrasound system that uses a custom complementary metal-oxide-semiconductor linear array detector. This novel sensor allows parallel phase-sensitive detection of very low contrast modulated signals with performance in each channel comparable to that of a discrete photodiode and a lock-in amplifier. Application of the instrument is demonstrated by parallelizing spatial measurements to produce two-dimensional thickness maps on a layered sample, and spectroscopic parallelization is demonstrated by presenting the measured Brillouin oscillations from a gallium arsenide wafer. This paper demonstrates the significant advantages of our approach to pump probe systems, especially picosecond ultrasonics.
 [doi:10.1063/1.3298606]

I. INTRODUCTION

Time-resolved picosecond laser ultrasonics (TR-PLU) is a nondestructive pump/probe technique.[1–3] To generate ultrasound in TR-PLU, an ultrashort pump laser pulse is focused onto a substrate or sample, resulting in absorption and thermal expansion. This, in turn, launches an elastic strain pulse which can, for example, be used to penetrate thin films or nanostructures to measure material mechanical properties[4] or film thickness.[5] Ultrasound detection is performed by using an ultrashort probe beam pulse with variable delay to measure the slight change in the optical properties of the sample caused by reflected strain pulses as a function of time.

The convenience of PLU has improved in recent years as picosecond and femtosecond laser sources with adequate power and stability have become far more reliable and affordable. However, a major limitation to the wider use of TR-PLU remains the slow data acquisition arising from the very low contrast of the optical signals. This necessitates narrow band, phase-sensitive detection with a lock-in amplifier (LIA). Since a LIA is a single channel instrument, to obtain just one PLU measurement requires that a sequence of measurements is obtained as a function of probe beam time delay. Maximum acquisition rates are generally limited to several hundred samples per second by the LIA time constant, vibration, and the translation speed of mechanical stages, so obtaining images or spectra is very time consuming.

This paper demonstrates how highly sensitive, multichannel PLU data acquisition can be performed with a custom complementary metal-oxide-semiconductor (CMOS) array detector of our own design. We give examples of imaging and spectroscopy that is parallel of spatial and parallel wavelength data acquisition. The increase in acquisition rate will have a major impact on practical materials characterization with PLU and a wide range of other pump/probe techniques.

II. PARALLEL MEASUREMENT OF PLU SIGNALS

In common with most pump/probe and several other techniques, the optical signals encountered in PLU consist of a large dc background with a very low contrast modulated component (typically from 10^{-4} to 10^{-6} of the dc level) caused by the picosecond acoustic pulse. This necessitates large photon budgets. For example, to resolve a modulated signal that is 10^{-6} of the dc level, it requires the detection of a minimum of 10^{12} photoelectrons even in the best case when the signal is shot noise limited.

To overcome the effects of shot noise therefore requires a very high dynamic range and a low bandwidth (long integration times). If integration is performed at dc it is subject to drift and $1/f$ noise, so in a conventional PLU arrangement, the pump beam is intensity modulated, often with a mechanical chopper, and the probe beam is detected with a photodiode connected to a LIA. This allows for narrowband detection well away from $1/f$ and other low frequency noise sources.[5]

To implement parallel PLU requires a different approach as it is not feasible to use a large array of conventional LIAs. Various approaches to parallel phase sensitive detection have been implemented by our group[6] and others,[7,8] but none perform very well for PLU as they lack either the speed or the dynamic range to handle the necessary photon budget. Here, we use a custom CMOS sensor that has been specifically optimized for these types of measurements. These initial re-

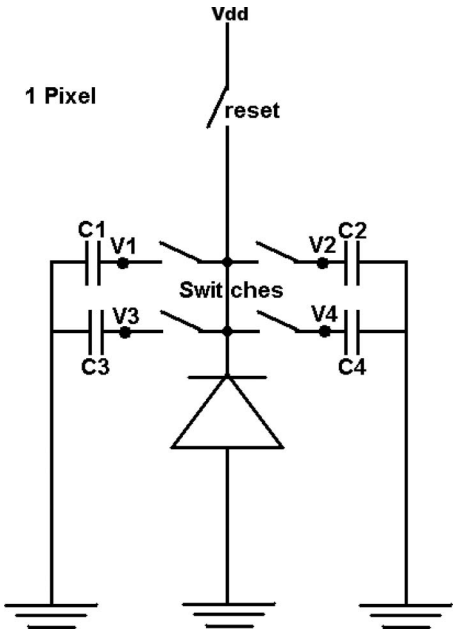

FIG. 1. Simplified pixel level schematic showing four independently switchable storage capacitors.

sults use a 1×64 pixel device, but a 1×256 version is currently in production and the design is scalable to higher resolutions.

A. Custom CMOS detector

The detection scheme consists of a custom CMOS linear detector array (1×64 pixels), a field programmable gate array providing control of logic and clocks and an analog-to-digital converter (ADC) under personal computer control. The array is a modified active pixel sensor design. In order to achieve the required photon budget, and hence noise performance, each pixel has four large independently shuttered capacitors to drastically boost the well capacity from that of the diode alone. This means that the sensor can obtain four synchronous images before any data need to be downloaded (see Fig. 1). This enables us to lock into frequencies well beyond the camera frame rate. The pixels are randomly addressable making the device flexible to use as low light level pixels can be read more frequently to improve their signal-to-noise ratio (SNR) without the requirement of reading out the entire array. Unlike commercially available large well detector arrays, the detector employs global shuttering, so all pixels are clocked in phase. This removes problems such as the amplitude/phase cross-talk introduced by the simpler rolling shutters generally employed by commercially available linear sensors.[9] The effective well capacity of each pixel in the CMOS array is approximately 600 Me^- allowing a potential shot noise limited sensitivity of 88 dB V for a single measurement acquired within one cycle of the pump beam intensity modulation. The large dynamic range requires an ADC with a bit depth of ~15 bits over the output voltage range of the device to keep the quantization noise below the shot noise level.

The array makes efficient use of available light due to a very high fill factor (light sensitive portion of the pixel) and negligible dead time. This arises because we use multiple storage capacitors which allow integration of one phase step (on one capacitor) while simultaneously reading out another phase step (stored in another capacitor). The continual integration, reset, and readout all take place within one modulation cycle and so no light is wasted. We use a standard four-step algorithm[10] to extract the ac parameters as below

$$\text{amplitude} = \sqrt{(S_3 - S_1)^2 + (S_4 - S_2)^2}, \tag{1}$$

$$\text{phase} = \arctan\left(\frac{S_3 - S_1}{S_2 - S_4}\right), \tag{2}$$

$$\text{dc} = \frac{S_1 + S_2 + S_3 + S_4}{4}, \tag{3}$$

where S_m=measured signal for step m.

The detector has high speed output amplifiers that can operate to at least 10 MHz, this means that we can operate the camera at ~40 kframes/s. Each frame corresponds to one complete modulation cycle and is related to the time it takes to acquire the data for all four phase steps for each of the 64 pixels. As the pixels are shuttered globally this is approximately equal to four integration periods (4×6.25 μs). We currently operate at 1.7 kframes/s (integration time per phase step is ~147 μs) due to the particular arrangement of our experiment. The precise details of this are given in Ref. 11.

B. Example applications

In the following sections we give two examples where we speed up the data acquisition by parallelization of (a) spatial information and (b) spectral information. In some cases where one is photon limited by available probe power, parallelizing the detection may not speed up the measurements. In the case of the laser ultrasound experiments described here, the optical power limitation arises from the possible damage to the sample if the pump pulse power density is too high. Spreading the pump power over multiple excitation points enables the generation of a larger integrated ultrasonic signal, thus allowing parallel detection to have a significant advantage over single point approaches.

1. Parallelizing spatial information

With simple modifications to the standard optical arrangement, the pump and probe beams can be brought to a line focus on the sample. Imaging this line onto the detector allows each pixel to measure a different spatial position on the sample. This arrangement allows sample thickness or acoustic velocity measurements over a line of a sample, and with a single "broom" sweep a two-dimensional area can be measured. This approach is suitable for analyzing multiple layer structures, through echo location, as well as transparent samples using the characteristic frequency of the produced oscillations.

The experimental arrangement is similar to that described in Ref. 9 with the addition of two weak cylindrical lenses to focus the probe and pump beams to a line of approximately 60×2.6 μm^2 (Fig. 2). The laser used is a Spec-

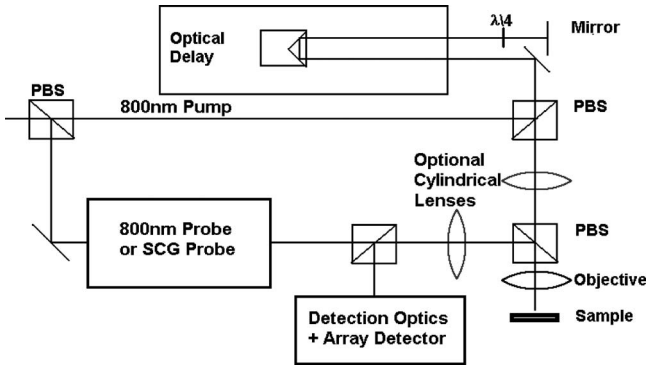

FIG. 2. Schematic of the experimental arrangement.

tra Physics Tsunami with <100 fs pulse width and a pulse repetition rate of 80 MHz, the pump and probe beam both have a wavelength of 800 nm, the linewidth of the pulse is ~ 30 nm. The pump beam was 100% modulated by a mechanical chopper at 1700 Hz to match the frame rate of the camera. The average optical power incident at the sample has been increased from the single point case to 230 mW for the pump beam. The probe power returning from the sample and imaged across the detector was approximately 60 μW. The sample consisted of a silicon substrate with a chromium overlayer with two regions of approximately 55 and 75 nm thick.

The demodulated probe signal consists of a large step change known as the coincidence peak, corresponding to zero delay between pump and probe, followed by a slow thermal relaxation. The signals due to the ultrasonic waves reflecting between the overlayer and the substrate are superimposed on this background.

The thermal background was removed by subtracting a curve fit to the experimental data, and high frequency noise due to vibrations or electronics was filtered. Figure 3 (top) compares the demodulated signal from a single pixel of the array to that acquired from a traditional single photodiode and LIA. The first three echoes are clearly visible. We obtained 80 averages from the array taking 112 s to acquire the data in the 64 channels. The single photodiode system acquired a single channel in 48.5 s. The chosen noise level for the comparison of the two detector approaches was approximately 5×10^{-6} of the dc level, this level allows the first three echoes to be seen clearly. Lower noise levels can be obtained by increasing the number of averages for the array or the integration time of the LIA. The lower part of Fig. 3 shows the data recorded by the whole array. Only the central 40 or so pixels are active due to low light level at the extremities of the line focus. In the current experiment using 80 averages we would expect the noise level to be 2.4×10^{-6} of the dc level if the wells were 95% full and shot noise was the only significant noise source. We are currently two times away from this, in practice, due to other noise sources, including, for example, laser flicker noise and vibrations, etc.

The imaged region of the sample had an overlayer of constant nominal thickness, so the temporal positions of the echoes are similar at all spatial positions. These temporal measurements can be converted to thickness values given the published value for the longitudinal velocity of chromium

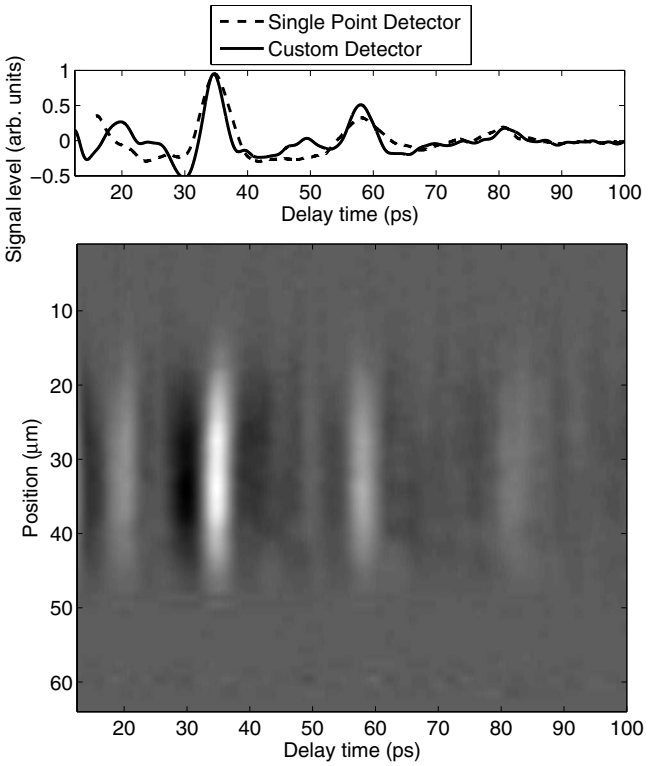

FIG. 3. Top: A single pixel from the array detector compared with a result from a single point detector for a thinly coated sample. Bottom: The acquired data from the array detector showing the multiple echo returns from the interface between the coating and the substrate.

(6608 m s^{-1}).[12] The thickness can be calculated by using the time between the coincidence peak and the first echo, or the time between subsequent adjacent echoes. The thickness derived from the time between echoes data will be more reliable as uncertainty in the exact position of the sound generation is removed. The absorption of the pump pulse takes place within the chromium leading to an offset in the zero time position. Time delays between subsequent echoes do not suffer from this problem; however, signal levels are lower and thus more susceptible to the influence of noise.

Using the delay between the coincidence peak and the first echo gives a mean thickness of 75.5 nm (σ=0.2 nm) for the central 32 pixels, whereas if the time between first and second echoes is used, we recover, as expected, a slightly larger thickness of 77.5 nm (σ=0.5 nm). A low spatial frequency variation in the thickness measured across the array is observed, with a standard deviation of 0.7 nm in the case of the measurement between the coincidence peak and the first echo. We believe that this is due to slight misalignment between the generation and detection optics. This misalignment does not significantly affect the ultrasonic probe measurements, but it does perturb the thermal propagation which slightly changes the position and shape of the coincidence peak. As we use the coincidence peak as our zero time reference any changes to this will cause an apparent change to the thickness of the layer.

The same measurement was performed across the transition between regions of different thickness, where additional averaging (250) allows clearer echo signals to be seen. The transition region is approximately 10 μm wide and is

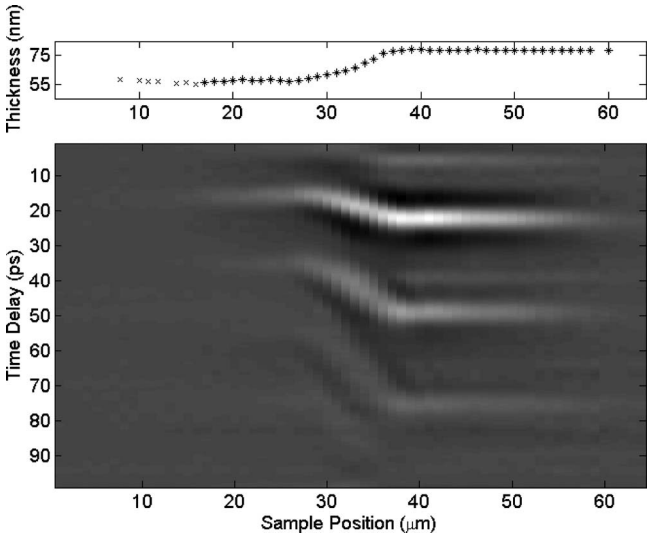

FIG. 4. Top: Thickness profile obtained from echo times and known acoustic velocity. Bottom: Echo returns from the interface between the coating and substrate between two regions of differing thickness.

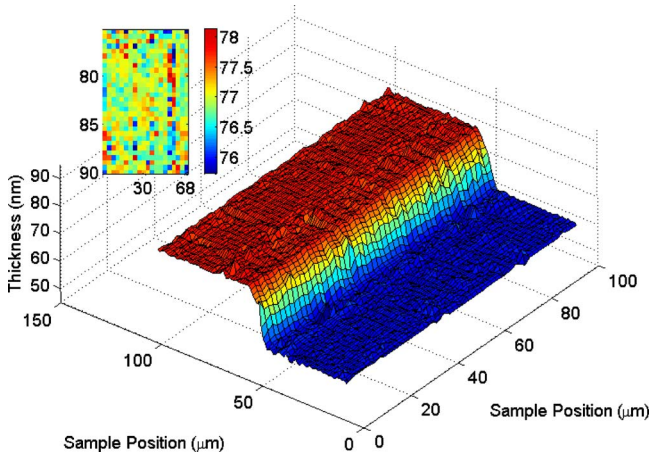

FIG. 5. (Color online) Coating thickness map over an extended region of the sample. Inset shows a zoom of a flat region where the standard deviation of the thickness is ~0.3 nm.

clearly resolved by the system (the optical resolution is 1.3 μm). Figure 4 (top) shows the thickness derived from the time between the second and first echoes (stars) and the lower part of the figure shows the data obtained with the custom detector. The echoes are again clearly visible even across the transition from one region to the other. The flat regions either side of the transition produce values for the thicknesses of 76 and 55 nm, which is consistent with atomic force microscopy measurements. The crosses in the top of Fig. 4 are the thickness values derived from the coincidence peak and first echo times as in this region the second echo data were not available. The offset error discussed earlier has been removed by comparing the first to second echo time with the copeak to first echo time for a pixel where the SNR was good. As long as 1 pixel has a good second echo signal this correction can be performed to remove the zero time ambiguity of the coincidence peak.

We currently acquire 1700 sets of data per second with the linear array detector, where each set contains data corresponding to four phase steps for each of the 64 pixels. This limitation is imposed by the data acquisition rate of the ADC card. With a point detector and similar signal noise, acquiring data equivalent to Fig. 2 would take 52 min, compared to 112 s with our array. This is approximately 28 times faster and the data are more robust since it is recorded in parallel. With some simple modifications, such as a faster ADC card, a faster optical delay stage and increasing the probe beam intensity, an increase in data acquisition speed of additional factor of 4 times is readily achievable. The ADC unit used for this experiment was 18 bits deep and was the main limitation on the data acquisition speed, a faster ADC with bit depth of 16 should increase the data acquisitions speed by a further factor of 4.

This significant increase in the data acquisition speed allows the mapping of sample properties, in this case coating thickness, over an extended region. Figure 5 shows a thickness map across the transition region over an area of ~100 $\times$100 μm^2, this image took 2 h and 45 min to acquire and the thicknesses are derived from the first echo locations (this would take approximately 3 days to acquire with the single point detector). The transition is well resolved and the regions either side appear very uniform. This uniformity is highlighted in the inset, which shows a rescaled image of a 60$\times$20 μm^2 region of the thicker part of the coating, the standard deviation of the thickness values of this region is 0.3 nm.

The parallel technique discussed here has made over an order of magnitude improvement in data acquisition time compared to our conventional point detector. In addition, the detector array we have developed is scalable to larger dimensions this combined with faster ADCs will allow even greater improvements in the future.

2. Parallelizing spectroscopic information

This section considers parallelizing spectral information. Measuring the interaction of different probe wavelengths can yield important information about the sample under study, it is of particular interest for investigation of the wavelength dependence of the shape of the acoustic echoes reported in some PLU studies.[13,14] This effect is believed to be related to electronic interband transition effects.[13] Multiple probe wavelengths have been used to investigate the relative importance of generation mechanisms (electronic or thermal effects) for long lived coherent acoustic phonons in single crystal GaN.[15] These measurements have hither to been obtained with point measurement where a part of the source is scanned across a grating, this means that much of the detected power is wasted, so parallel detection of the available probe wavelengths greatly speeds up the measurement.

Incorporating a supercontinuum source[16] into the probe arm and a grating/lens before the linear array detector allows the possibility of parallel picosecond spectroscopy. Single point measurements using a supercontinuum probe beam on GaAs have been presented by Rossignol *et al.*;[17] however, in this case, the signal from each wavelength was recorded separately by preselecting with optical filters at the output of the supercontinuum fiber or before the photodiode and detecting the reflected light using a photodiode and LIA. We

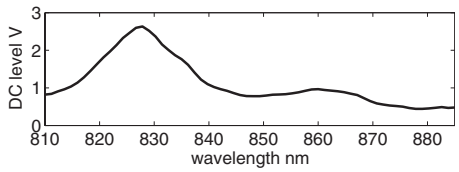

FIG. 6. The portion and intensity of the optical wavelengths from the output of the SCG probe beam used in the experiment.

present the detection of 64 wavelengths simultaneously on GaAs with a probe beam optical bandwidth of ~75 nm.

The system setup is shown in Fig. 2, the probe beam is now derived from the output of a supercontinuum fiber (SCG) and the line imaging lenses are removed. The fiber used was a Newport SCG-800 Photonic Crystal fiber and a ×20 objective lens was used to couple the input beam (input power of ~400 mW, ~100 fs pulse width, and input wavelength of 800 nm) into the fiber, a ×10 objective lens was used
to recollimate and expand the broadband output beam (~120 mW). Both the pump and a portion of the probe beam are focused onto the same point on the sample.

A selection of the output spectrum is shown in Fig. 6. The highly nonlinear fiber modifies the 800 nm input pulse into a broad spectrum output pulse, primarily via self-phase modulation.[18] This gives an output spectrum covering roughly 500–1200 nm. A portion (limited by the choice of optics/coatings in the system) of this range of wavelengths after returning from the sample is spread across the CMOS detector using a 300 lines mm^{-1} diffraction grating and a 50 mm focal length lens (see Fig. 6). The pump beam had a pulse energy of ~0.5 nJ and the probe beam contained ~1.5 nJ in total across the entire broadband spectrum. The supercontinuum probe beam is focused to the same location of the sample as the 800 nm pump beam and the returning light is then dispersed by a diffraction grating and focused into a line by a lens onto the linear array detector. The detector integrates the detected probe light to produce four samples per modulation cycle. These are used to obtain the amplitude and phase at the modulation frequency as before. Although these measurements do not use a significant amount of the available bandwidth from the supercontinuum fiber, it is considerably wider than the 28 nm bandwidth obtainable from the laser directly.

The sample used in this example was GaAs, which is semitransparent for the range of wavelengths used. The change in the reflectivity of the probe beam will be oscillatory in nature due to the interference between the surface of the sample and the refractive index perturbation produced by the propagating sound wave. The propagation of the acoustic wave causes the phase of the light reflected by the sound wave to change, this leads to an oscillating signal $S(x)$, the so-called Brillouin oscillations:[19] see Eq. (4) below, where a is the dc level, b is the modulation depth, f_b is the Brillouin frequency, and ϕ is the initial phase of the oscillations. The frequency of the oscillations is given by Eq. (5) below, where n is the real part of the refractive index, v_a is the acoustic velocity, λ is the wavelength, and ϑ is the angle of incidence of the probe beam which is usually zero in our case,

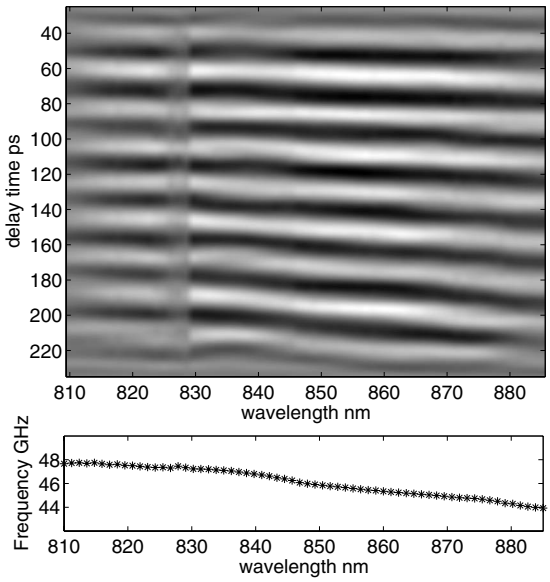

FIG. 7. Top: The measured Brillouin oscillations for different probe wavelengths. Bottom: The corresponding Brillouin frequencies.

$$S(x) = a + b\,\sin[2\pi f_b(\lambda)x + \phi], \tag{4}$$

$$f_b = \frac{2v_a n}{\lambda}\cos\,\vartheta. \tag{5}$$

If the signal is truncated to remove the coincidence peak and the slow thermal relaxation is removed via fitting, an oscillating signal is obtained. Figure 7 shows the signals obtained for all of the pixels of the array and their corresponding Brillouin frequency. Good agreement is obtained across the entire range with the theoretical frequency using published values for n and v.[20]

We have demonstrated the acquisition of the signals for 64 wavelengths simultaneously over a range of ~75 nm. Recording the information in parallel produces a more robust set of data as each set of data is obtained in the same experimental environment reducing the impact of thermal drift and laser power variations.

C. Discussion

This paper has demonstrated the significant advantages of our "parallel detection" approach for picosecond laser ultrasonics, however, many pump/probe systems should also benefit from the detection technique described here. For example, Othonos *et al.*[21] studied the ultrafast carrier relaxation in InN nanowires by performing femtosecond differential absorption spectroscopy measurements. Here they used the pump probe technique, where the modulated pump pulse is used to excite the material; by probing the sample after the excitation with different probe wavelengths they investigated the effect on the optical properties of the sample as the photogenerated carriers relax. The change in the optical properties is related to change in the electronic structure of the sample caused by the pumping beam. Although not ultrasonic, this experiment uses essentially the same setup as in Fig. 2, just working on shorter time scales (a few picoseconds) and with more intense pump pulses for the carrier gen

eration. Similarly, Lupo *et al.*[22] investigated the ultrafast hole dynamics in nanocrystals, where they investigated the differences in the ultrafast absorption spectra for different nanodots and rods. In this experiment both the pump and probe wavelengths are changed and the spectra for different time delays are measured.

The flexibility of the detector means that it can operate in different modes to allowing it to operate over a wider range of applications. For example, changing the shuttering scheme of the detector allows correlated double sampling to be performed or the four storage capacitors could be all connected together to create a single large well allowing the device to be a drop in replacement for many commercially available integrating linear array detectors, but with bigger wells and faster operation.

In future chips we intend to use a variable gain so different light levels can be measured. This addition will allow the device to be shot noise limited over an extended range of illumination conditions. For low light conditions, the signal voltages are small and in these cases readout noise can dominate. Amplifying the signals before readout to the ADC overcomes this issue. The device is currently only shot noise limited when the wells are 50% full.

Other approaches are presently becoming available to increase the measurement speed of pump/probe systems and involve "locked" laser sources, where the pulse repetition rate of the two sources differ by a small amount (hertz to kilohertz).[23] This can greatly speed up measurements for pump/probe measurements including PLU by removing the need to scan a mechanical delay line. The parallelization described here is entirely compatible with these locked lasers (using delay repetition rates of <100 Hz) and it is likely the combination of these approaches will make pump/probe methods applicable for many applications which have been, hitherto, impractically slow.

[1] C. Thomsen, H. T. Grahn, H. J. Maris, and J. Tauc, Phys. Rev. B **34**, 4129 (1986).
[2] O.B. Wright, T. Hyoguchi, and K. Kawashima. Jpn. J. Appl. Phys., Part 2 **30**, L131 (1991).
[3] B. Perrin, B. Bonello, J. C. Jeannet, and E. Romatet, Physica B **219–220**, 681 (1996).
[4] E. Romatet, B. Bonello, R. Gohier, J. C. Jeannet, and B. Perrin, J. Phys. IV **06**, C7-143 (1996).
[5] O. B. Wright, J. Appl. Phys. **71**, 1617 (1992).
[6] I. R. Hooper, J. R. Sambles, M. C. Pitter, and M. G. Somekh, Sens. Actuators B **119**, 651 (2006).
[7] E. Beaurepaire, A. C. Boccara, M. Lebec, L. Blanchot, and H. Saint-Jalmes, Opt. Lett. **23**, 244 (1998).
[8] H. Chouaib, M. E. Murtagh, V. Guenebaut, S. Ward, P. V. Kelly, M. Kennard, Y. M. Le Vaillant, M. G. Somekh, M. C. Pitter, and S. D. Sharples, Rev. Sci. Instrum. **79**, 103106 (2008).
[9] R. J. Smith, M. G. Somekh, S. D. Sharples, M. C. Pitter, I. Harrison, and C. Rossignol, Meas. Sci. Technol. **19**, 055301 (2008).
[10] K. Creath, Prog. Opt. **26**, 349 (1988).
[11] R. A. Light, R. J. Smith, N. S. Johnston, S. D. Sharples, M. G. Somekh, and M. C. Pitter, Proc. SPIE **7570**, 7570 (2010).
[12] G. Kaye and T. Laby, *Tables of Physical and Chemical Constants*, 15th ed. (Longman, London, 1986).
[13] A. Devos and C. Lerouge, Phys. Rev. Lett. **86**, 2669 (2001).
[14] A. Devos and R. Cote, Phys. Rev. B **70**, 125208 (2004).
[15] S. Wu, P. Geiser, J. Jun, J. Karpinski, and R. Sobolewski, Phys. Rev. B **76**, 085210 (2007).
[16] Newport supercontinuum fibre module, SCG-800 photonic crystal fibre.
[17] C. Rossignol, J. M. Rampnoux, T. Dehoux, S. Dilhaire, and B. Audoin, Rev. Sci. Instrum. **77**, 033101 (2006).
[18] F. G. Omenetto, N. A. Wolchover, M. R. Wehner, M. Ross, A. Efimov, A. J. Taylor, V. V. R. K. Kumar, A. K. George, J. C. Knight, N. Y. Joly, and P. S. J. Russell, Opt. Express **14**, 4928 (2006).
[19] C. Thomsen, H. T. Grahn, H. J. Maris, and J. Tauc, Opt. Commun. **60**, 55 (1986).
[20] S. Adachi, in *Properties of Aluminium Gallium Arsenide*, edited by S. Adachi (INSPEC, London, 1993), pp. 22–23.
[21] A. Othonos, M. Zervos, and M. Pervolaraki, Nanoscale Res. Lett. **4**, 122 (2009).
[22] M. G. Lupo, F. Della Sala, L. Carbone, M. Zavelani-Rossi, A. Fiore, L. Luer, D. Polli, R. Cingolani, L. Manna, and G. Lanzani, Nano Lett. **8**, 4582 (2008).
[23] A. Bartels, R. Cerna, C. Kistner, A. Thoma, F. Hudert, C. Janke, and T. Dekorsy, Rev. Sci. Instrum. **78**, 035107 (2007).